

EXPERIMENTS AND MODELING OF PARTICULATE DEBRIS SPREADING IN A POOL

A. Konovalenko, S. Basso and P. Kudinov

Division of Nuclear Power Safety
Royal Institute of Technology (KTH)
Roslagstullsbacken 21, D5, Stockholm, 106 91, Sweden
kono@kth.se; simoneb@kth.se; pkudinov@kth.se

S. E. Yakush

Institute for Problems in Mechanics of the Russian Academy of Sciences
Ave. Vernadskogo 101 Bldg 1, Moscow, 119526, Russia
yakush@ipmnet.ru

ABSTRACT

Melt fragmentation, quenching and long term coolability in a deep pool of water under reactor vessel are employed as a severe accident mitigation strategy in several designs of light water reactors. Success of the strategy is contingent upon effectiveness of natural circulation in removing the decay heat generated by the porous debris bed. Geometrical configuration of the bed is one of the factors which affect coolability of the bed. Boiling and two-phase turbulent flows in the pool serve as a source of mechanical energy which can affect the initial geometry as well as dynamically change the shape of already formed debris bed.

The main goal of this work is to provide experimental data on spreading of solid particles in the pool by large scale two-phase flow structures induced by gas injection from the bottom. These data are necessary for development and validation of predictive capabilities of computer codes allowing numerical modeling of the debris bed formation at prototypic severe accident conditions. In PDS-P experiments air injection at the bottom of the test section is employed in order to create large scale flow in the pool. The test section is constructed as a rectangular tank. It has close to 2D geometry with fixed width (72 mm), variable length (up to 1.6 m) and allows water filling depth of up to 1 m. The variable pool length and depth allows formation of the different in size and pattern two-phase circulating flows. Experimental conditions such as gas-phase flow rate and particle properties (density and size) are scaled to maintain relevancy to the prototypic accident conditions. The average void fraction in the pool is determined by video recording and image processing. Particles are supplied from the top of the facility above the water surface. In the separate-effect studies of the influence of two-phase currents on particle trajectories and bed formation, a low particle flow rate is required in order to minimize or completely exclude particle-particle interaction. Results of several series of PDS-P (Particulate Debris Spreading in the Pool) reported in this paper are analyzed analytically. The preliminary scaling approach is proposed and has good agreement with experimental findings.

KEYWORDS

Particulate spreading, debris bed formation, three-phase flow, turbulence in the pool.

1. INTRODUCTION

In a Nordic BWR type reactors the lower drywell flooded with water is the last barrier to prevent basemat penetration and escape of fission products into environment in a hypothetical severe accident (SA) with molten corium released from the reactor vessel (RV). Being discharged into several meters deep water pool, the molten corium debris is subject to fragmentation and quenching. The fragmented particles sedimentation process leads to a formation of a porous debris bed on the pool basemat. The corium debris bed re-melting by the decay heat can be avoided if the latter is removed by the natural circulation of the coolant. Both the theoretical advances, the developed codes [1] [2] and experimental studies [3] used in their validation, have been performed in order to determine time scale of the dryout as well as its influencing factors such as: properties of the debris bed (particles size, bed porosity, bed geometry, etc.) and SA scenario conditions (e.g. system pressure). A typical geometry of the formed debris bed is a mound. The performed studies suggested that geometrical configuration of the debris bed is one of the main factors influencing the bed coolability. A tall debris bed can be hardly coolable and, in contrast, the same mass of the corium material can be easily cooled if the debris is spread uniformly over the whole available basemat area [1].

The shape of the debris bed is affected by particle transport:

- i. after settlement on the debris bed;
- ii. in the water pool above the bed.

Debris bed self-leveling occur due to mechanical energy originated from the coolant boiling in the porous bed. It should be noted that the pool can remain mostly subcooled in some reactor accident scenarios, it is quite possible that boiling will start rather early in the top part of the hot water plume stemming from the debris bed when hot water will approach to the surface and its temperature can exceed local saturation temperature according to the hydrostatic head. This effect was demonstrated in [4].

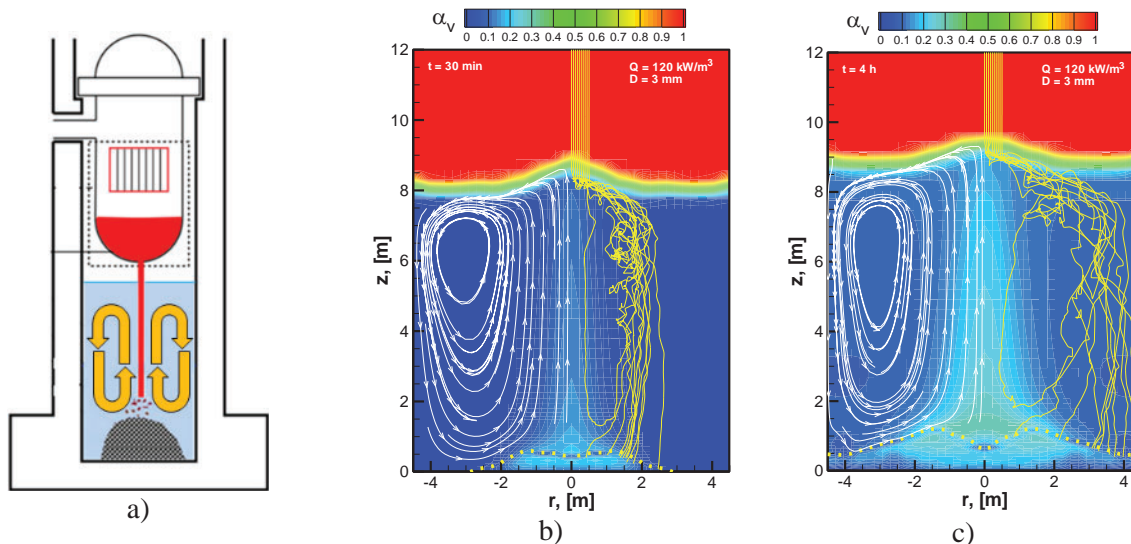


Figure 1: Illustration of the large turbulent currents during corium debris release in RV cavity under SA conditions (a) and simulation of particle trajectories affected by the circulation in the saturated pool at 30 min (b) and 4h (c), after [2]. See explanation in the text.

The effectiveness of the particulate debris bed spreading has been considered in experimental and theoretical studies [5] [6] [7] [8] [9] [10]. As experimental studies showed the debris self-leveling occurs due to particle motion at the top layer of the debris bed [8]. The large scale turbulent flows (as illustrated in Figure 1a) may affect the particle lateral spreading over the basemat [2] preventing formation of a tall debris bed. Smaller particles are more effectively spread by the flow. In Figure 1(b-c) from [2] the flow

field (white lines on the left), void distribution (color map), particle trajectories (yellow lines) and bed shape (dashed line) are presented for simulation time 30 minutes and 4 hours. The debris bed is spread over the bottom of the pool, despite the fact that all particles are released from a relatively small source in the center.

The goal of this work is to provide experimental data on particle spreading in the pool by large scale two-phase flow currents induced by gas injection at the pool bottom. The data are necessary for development and validation of predictive capabilities of computer codes for modeling of the debris bed formation at prototypic severe accident conditions. In this paper we also develop a scaling approach which has been validated against obtained experimental data.

2. EXPERIMENTAL APPROACH

In the experiments we quantify distribution of the particles along the pool bottom as a function of the gas injection parameters. The technique is similar to that used in studies on self-leveling and spreading of the particulate debris bed in PDS-C (closures) facilities reported in [8] and [9]. A detailed description of the measurements technique is reported in [11]. The test conditions and measured parameters for the new series of the tests are given below.

2.1 PDS-P facility and test conditions

The PDS-P (particulate debris spreading in the pool) facility consists of following main parts: the particle delivery system, main water tank, the particle collection system, gas supply and flow rate measurement system [11]. The general view of the facility is illustrated in Figure 2(a) as well as snapshot in operation in Figure 2(b). With upgraded PDS-P facility the reported herein tests were performed with following varied and fixed parameters (see Figure 2 for definition of some parameters). Depth of the water pool H_{pool} is either: 0.5¹; 0.7 or 0.9 m. Length of the pool L_{pool} is either: 0.5; 0.9 or 1.5 m. Fixed tank width: 72 mm. Gas injection chamber with adjustable air mass flow rate Q_g within range of: 0.26-0.7 g/s. Low particle delivery flow rate ranging between 1 and 5 g/s. Particles used in experiments reported herein:

- Stainless steel spheres 3 mm in diameter (SSs_S3) and with $\rho_{p,SS3} \cong 7.8 \text{ g/cm}^3$;
- Glass spheres 3 mm in diameter (GLs_S3) and density $\rho_{p,GL3} \cong 2.6 \text{ g/cm}^3$;
- Stainless steel spheres 1.5 mm in diameter (SSs_S1.5) and density $\rho_{p,SS1.5} \cong 7.8 \text{ g/cm}^3$.

This dimension is chosen in order to preserve close to 2D geometry for the turbulent currents and particles spreading, i.e. pool width is much less than length and height of the pool. On the other hand the pool width should be kept much larger than the characteristic particle size (1.5-3 mm vs 72 mm in reported tests here) in order to minimize influence of the particle-wall interaction. The water tank is made of acrylic material having wall thickness of 20 mm. A few pairs of rigid bars are installed as shown in Figure 2 to minimize vibrations and bulging of the tank walls during air injection.

Particle catchers are installed to be accessible outside the tank. A single catcher consist of: catcher wall separator, small funnel (Figure 2b), quick coupler (black components attached to the tank bottom in Figure 2a) and 50 mm diameter hose. The longest hoses (0.5 m) are positioned near the gas injection chamber where a largest mass fraction of the particle material is expected. The distances between the

¹ Note, tests with particles have not yet been performed for $L_{pool} = 0.5 \text{ m}$ long pool.

catcher's walls is 10 cm. The first catcher (Figure 2a) also collects particles which fall on the gas injection plate and thus has total effective length of 30 cm.

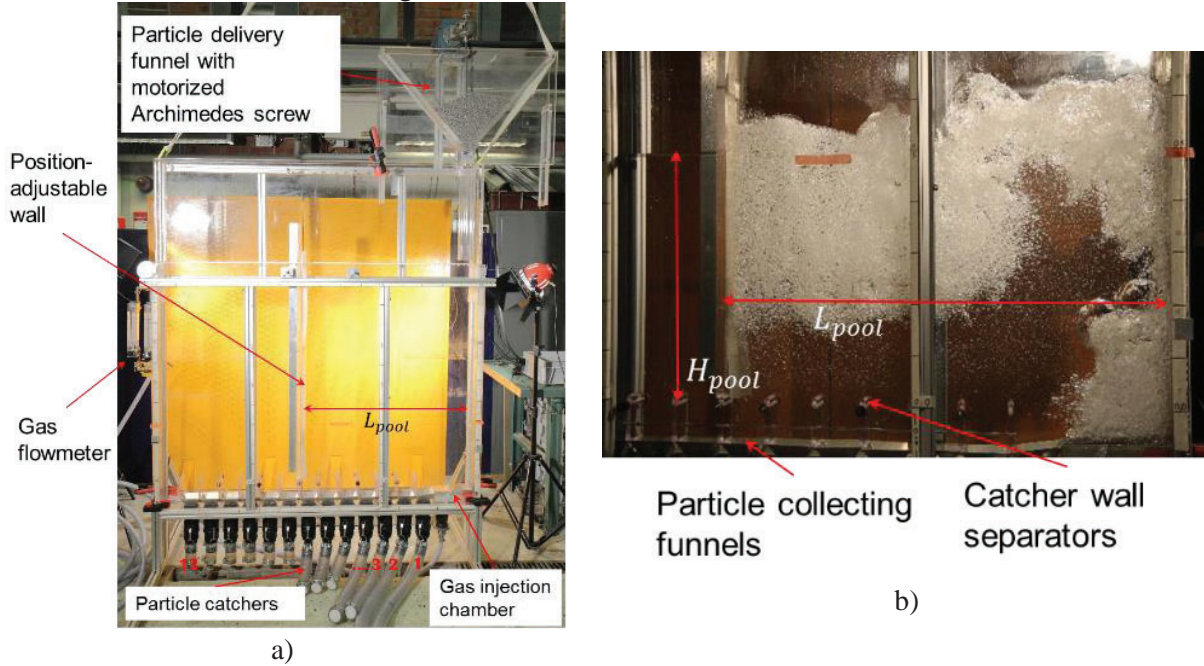


Figure 2: PDS-P facility: general view (a) and test section in operation (b). The pool depth H_{pool} (b) is measured from the upper tip of the walls separating particles catchers.

3 RESULTS AND DISCUSSIONS

3.1 Test conditions

In this work we report 34 two-phase flow tests (without particles) and 63 tests performed with low particle delivery rate. The gas chamber is positioned at one side of the water pool, instead of central position in previous tests [11].

3.2 Tests without particles

The comparison of the tests without particles and with gas injection in the center and aside is shown in Figure 3. We followed the same image processing technique [11] to determine total void fraction α as an average from five snapshots of the pool. Note that relatively large error bars in Figure 3 can be attributed to the small number of images used in the processing. Thus it is believed that provided error is overestimated. We found that total void fraction in the pool is different for the tests where ratio H_{pool}/L_{pool} is the same but the H_{pool} and L_{pool} values are different. For example two out of several cases when $H_{pool}/L_{pool} = 0.5/0.497 \approx 0.9/0.894 \approx 1.01$. Therefore, we interpolate the total void fraction by the following analytical representation where both dimensions of the pool are separate variables:

$$\alpha = a \cdot L_{pool}^b \cdot H_{pool}^c \cdot Q_g^d, \quad (3.1)$$

$$a = 0.052, b = -0.818, c = -0.197, d = 0.474,$$

where $a \dots d$ are fit constants, α ranges within $[0; 1]$, Q_g is expressed in g/s and pool dimension are in meters. The quality of this fit is illustrated in Figure 4. As seen, the maximum deviation from the experimental values lies below 10% in measured void fraction. The gas mass flow rate exponent d is comparable to the value of 0.5 determined previously [11] for the symmetric pool-centered gas injection.

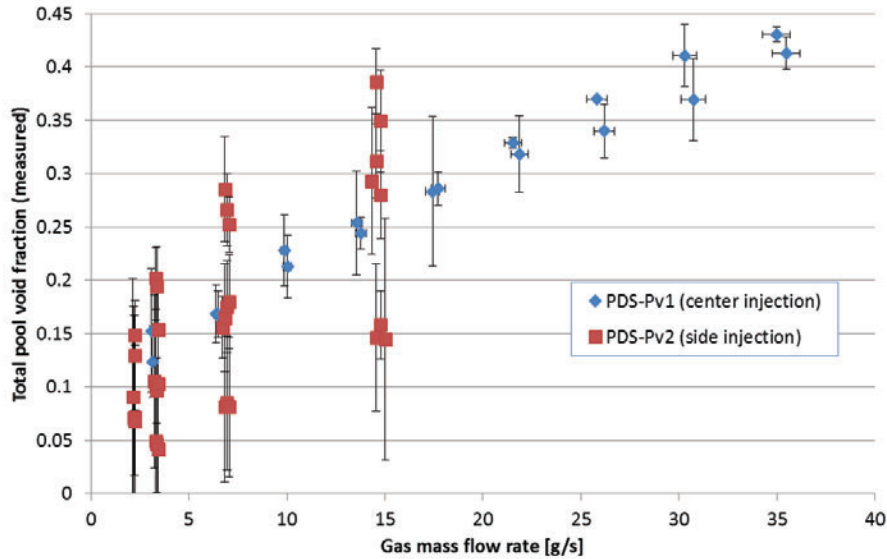


Figure 3: Measured total void fraction in the pool for tests without particles (two-phase flow). The measurement error of the gas flow rate does not exceeds 2% (horizontal error bars are not shown).

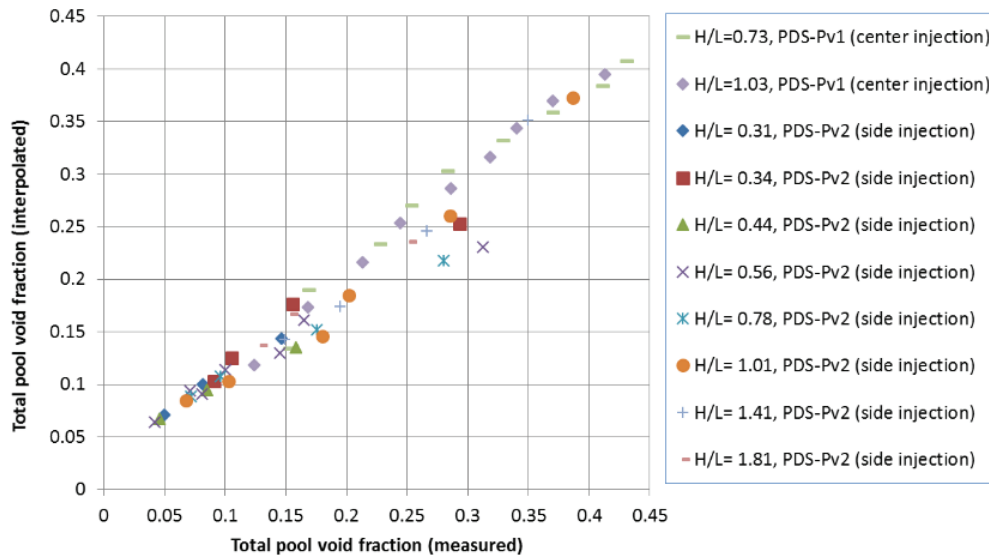


Figure 4: Interpolated void fraction versus experimentally measured values. Short notation H/L in the legend is the ratio of the pool depth to its length H_{pool}/L_{pool} .

The estimated total void fraction α is an integral quantity characterizing the turbulent two-phase flow in the pool. Another characteristics which can be easily estimated in our tests is an effective void fraction α_{eff} . It is defined as an average void fraction within active pool zone where two-phase flow (bubbles) are visually observed. Typically it is an upper half and right side (above injection plate) of the pool as shown in Figure 2(b). The same image processing procedure (as to determination of the total void fraction) has been applied where area of the active zone is estimated. The comparison of the α_{eff} versus α experimentally measured values are shown for all side-injection experiments in Figure 5. As seen from

the graph the effective void fraction can be ~10% higher than the total one in the pool. The highest values are observed for the lowest pool dimensions ratio H_{pool}/L_{pool} . On the other hand, high gas flow rate causes $\alpha_{eff} \rightarrow \alpha$ i.e. void is present almost everywhere in the pool.

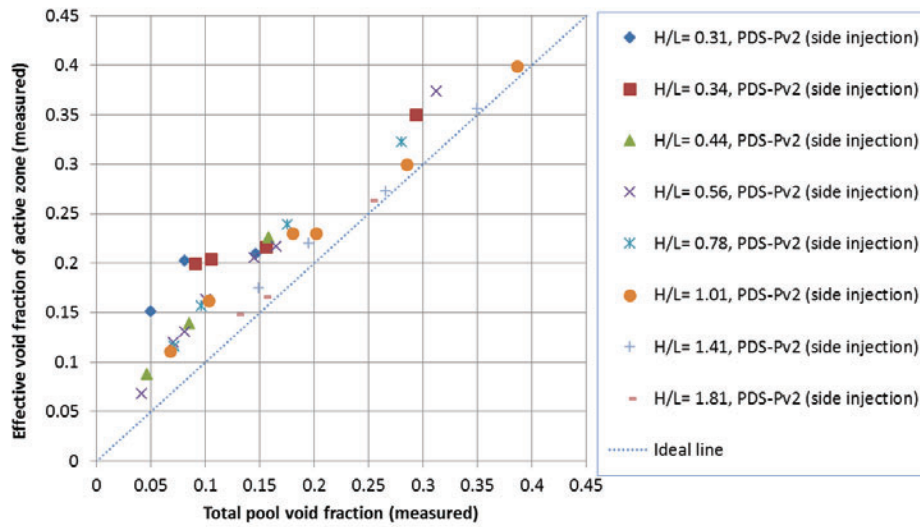


Figure 5: Comparison of the measured total vs effective void fractions in the pool.

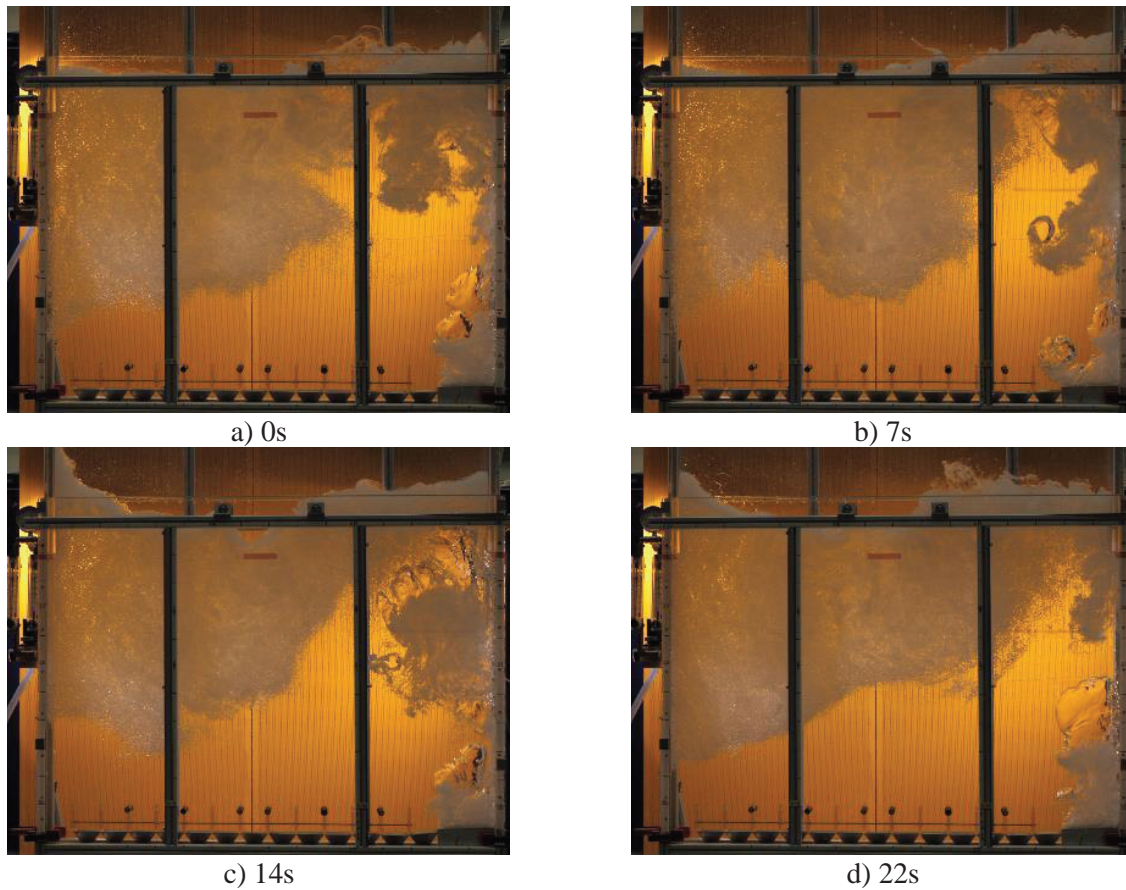


Figure 6: Snapshots of the particles-free test NOPs-28 with highest air flow rate of 15 g/s, $H_{pool} = 0.9$ m pool depth and $L_{pool} = 1.6$ m pool length. The relative to image (a) time offset in seconds of each snapshot is indicated below each subfigure.

Another remarkable feature of the flow is that at low gas injection rate a steady flow pattern and void distribution is observed whereas at high injection rates the pattern can change dynamically as shown in Figure 6. Large waves at water surface and the flow in the pool experience erratic oscillations. Large regions with near to 100% void fraction above injection chamber (Figure 6d) and regions with low void can be formed for short period of time. Such behavior is difficult to quantify in the experiment.

3.3 Tests with particles

In this work we consider the effects (Figure 7 through Figure 9) of (i) gas injection flow rate, (ii) particle diameter: 3 or 1.5 mm; (iii) particle density: glass or stainless steel; on particle spreading. The legend includes particle material, location of the gas injection, particle size, test number, height and length of the pool and gas injection flow rate. On the horizontal axis the particle catcher position r_i is normalized to the total length of the pool as r_i/L_{pool} . The mass fraction per catcher area on the vertical axis is non-dimension measure defined as:

$$\tilde{m}_i = \left(\frac{m_i}{M_{tot}} \right) / \left(\frac{A_i}{A_{tot}} \right), \quad M_{tot} = \sum_i m_i, \quad A_{tot} = \sum_i A_i, \quad (3.2)$$

where i^{th} catcher has area A_i , particle mass m_i . As seen from the figures, a small 1.5 mm (Figure 9) or light glass (Figure 8) particle spread more effectively than largest 3 mm stainless steel particle (Figure 7).

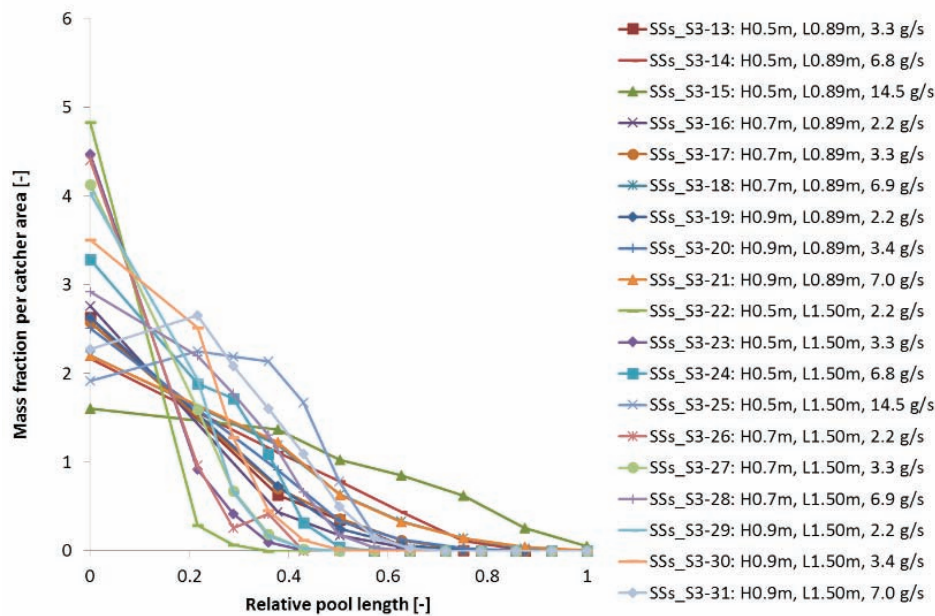


Figure 7: Spatial particle mass distribution from tests performed with 3 mm stainless steel particles.

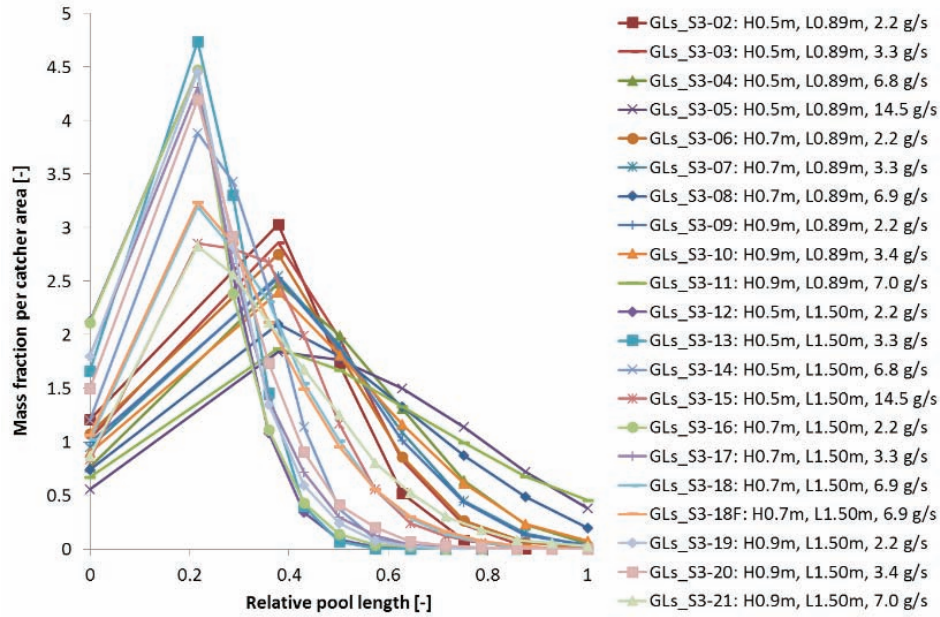


Figure 8: Spatial particle mass distribution from tests performed with 3 mm glass particles.

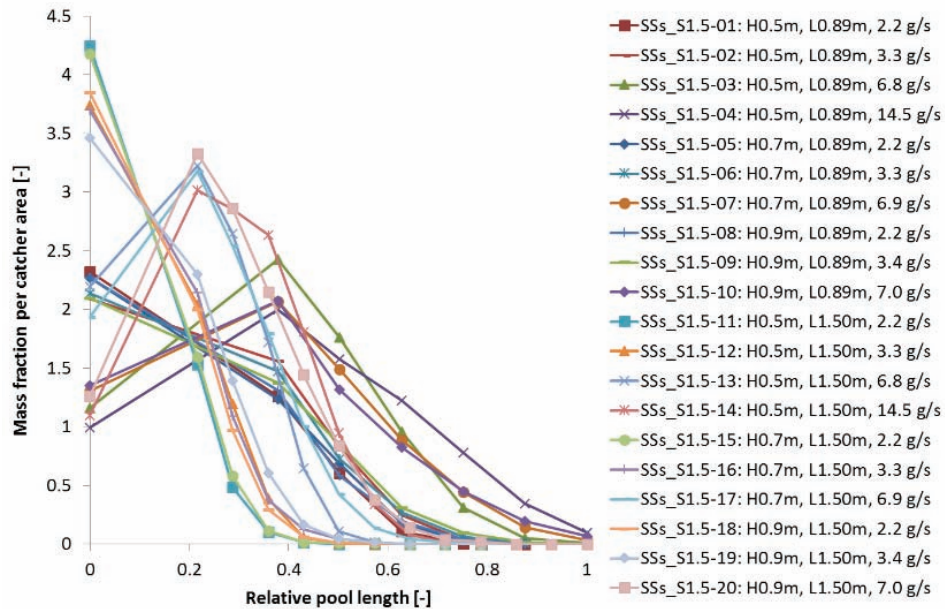


Figure 9: Spatial particle mass distribution from tests performed with 1.5 mm stainless steel particles.

3.4 Generalization of experimental data

Conditions of the tests are changed one parameter at a time in order to analyze separate effects by comparing the tangent of characteristic spreading angle $\tan \phi$ (see Figure 10)

$$\tan \phi = \frac{R_c}{H_{pool}}, \tag{3.3}$$

where R_c is center of mass of the debris collected in all catchers:

$$R_c = \frac{\sum_i m_i \cdot r_i}{\sum_i m_i} \quad (3.4)$$

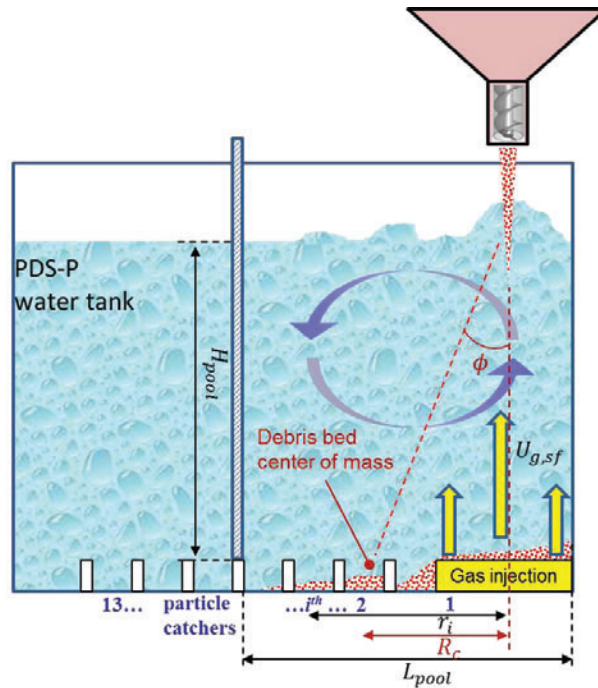


Figure 10: Schematics of the particle spreading in the PDS-P pool with defined characteristic spreading angle $\phi = \tan^{-1} \frac{R_c}{H_{pool}}$ depending on center of mass R_c (or average spreading distance R_{spr}) and pool depth H_{pool} .

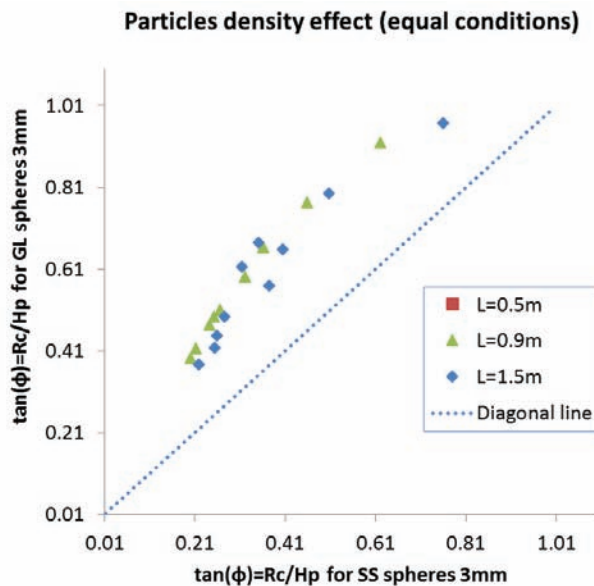


Figure 11: Particle density effect: comparison of the average spreading angle of the corresponding experiments performed at equal test conditions except for the density of the particles (glass vs stainless steel).

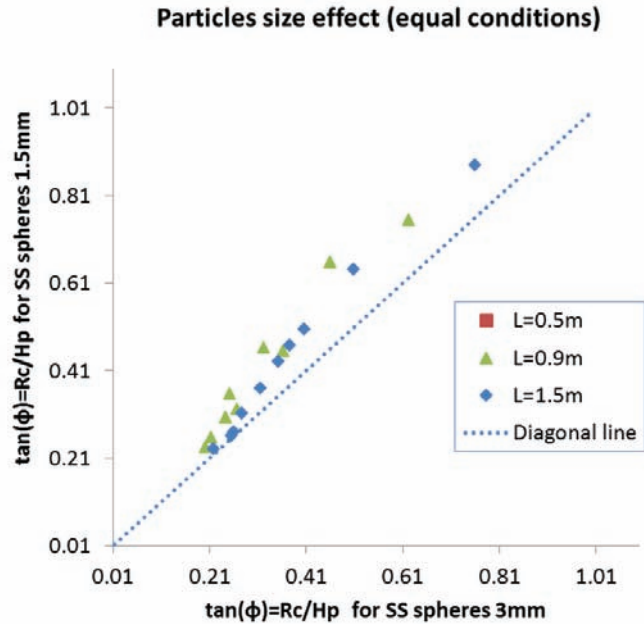


Figure 12: Particle size effect: comparison of the average spreading angle of the corresponding experiments performed at equal test conditions except for the size of the particles (1.5 mm vs 3 mm).

In Figure 11 tests with the 3 mm in diameter glass and stainless steel particles are compared to show the effect of particle material density. The effect of the particle size is similarly illustrated in Figure 12. The particle of different sizes exhibit the same spreading at low gas flow rates (few points laying on the diagonal at $\tan \phi \cong 0.21..0.25$ in Figure 12). In both cases (effects of the density and size) at high gas flow rates the effects of size and density becomes unimportant (upper right end of the plots in both figures). Comparing Figure 11 and Figure 12 one can conclude that particle density has stronger influence on particle spreading than particle size.

3.5 Scaling approach

In order to describe spreading of non-interacting particles caused by the large turbulent two-phase flows in the pool, we propose an empirical scaling approach. Consider a droplet of diameter d_p falling in the water pool of depth H_p . The terminal velocity of falling droplet U_t is evaluated from the balance of gravity and drag forces:

$$U_t = \sqrt{\frac{4}{3C_d} \frac{\rho_p - \hat{\rho}_c}{\hat{\rho}_c} g d_p}, \quad (3.5)$$

where ρ_p is particle density, $\hat{\rho}_c$ is modified coolant density $\hat{\rho}_c = (1 - \alpha)\rho_c$ and the drag coefficient C_d is a function of particle Reynolds number. The void fraction α is determined from the analysis of the tests without particles depending on pool dimensions and gas flow rate (3.1). For high particle Reynolds numbers it can be assumed that $C_d \approx 0.45$. The particle-water interaction time in the pool is then proportional to $t_{int} \propto H_p/U_t$. For a plane pool, the characteristic flow circulation time t_{circ} can be introduced as a ratio of the flow path (perimeter) to gas superficial velocity $U_{g,sf}$:

$$t_{circ} \propto \frac{2(L_p + H_p)}{U_{g,sf}} = \frac{H_p}{U_{g,sf}} \left(1 + \frac{L_p}{H_p} \right). \quad (3.6)$$

On the other hand, the characteristic horizontal velocity of the flow is:

$$v_{hor} \propto \frac{L_p}{t_{circ}}. \quad (3.7)$$

It can be assumed that the average horizontal distance R_{spr} by which a falling particle will be transported by the circulation flow is proportional to:

$$R_{spr} \propto v_{hor} \cdot t_{int} \propto U_{g,sf} \cdot \frac{L_p}{L_p + H_p} \cdot \frac{H_p}{U_t} = \left(\frac{U_{g,sf}}{U_t} \right) \cdot \frac{L_p H_p}{L_p + H_p} \quad (3.8)$$

or, the average tangent of the “spreading cone” angle ϕ (see Figure 10) is:

$$\tan \phi = \frac{R_{spr}}{H_p} \propto \frac{U_{g,sf}}{U_t} \cdot \frac{L_p}{L_p + H_p} = \left(\frac{U_{g,sf}}{U_t} \right) \cdot \frac{1}{1 + \chi}, \quad (3.9)$$

where $\chi = H_p/L_p$ is the ratio of the pool dimensions. We use following regression analysis

$$\tan \phi = F \left(\frac{U_{g,sf}}{U_t} \right) \cdot G \left(\frac{1}{1 + \chi} \right), \quad (3.10)$$

where, for the sake of simplicity, we choose both unknown functions $F()$ and $G()$ to follow power law with exponents $c_1 \dots c_3$:

$$\tan \phi = c_1 \cdot \left(\frac{U_{g,sf}}{U_t} \right)^{c_2} \cdot \left(\frac{1}{1 + \chi} \right)^{c_3}. \quad (3.11)$$

To validate Eq. (3.11) we analyzed the experimental data and assumed that the measurable center of mass of the debris bed (3.4) can be used as the average lateral particle spreading distance (3.8), i.e. $R_{spr} = R_c$. In the performed regression analysis we determined the unknown fit coefficients used in (3.11):

$$c_1 = 1.0000, c_2 = 0.4814, c_3 = 0.8537. \quad (3.12)$$

Remarkably, the exponent c_2 for the velocities ratio is close to 0.5 and exponent for the gas flow rate in the empirical expression for the total void fraction of the pool (3.1). The results of the regression analysis are shown in Figure 13. The average spreading of the stainless steel particles having 1.5 and 3 mm diameter is described very well by (3.11), with about 10% maximum deviation from the experimental values. However, the glass particles (red squares in Figure 13) can deviate up to about 20%. These type of particles spread on average better than Eq. (3.11) predicts. This effect can be explained by more effective bubble-particle interaction for light particle than for the heavy ones. We observed in experiments that after glass particles residing in the pool can be entrained by the turbulent flow for a long time ranging from tens of seconds up to few minutes after particles delivery is stopped. Further analysis and tests are required to clarify this effect as well as to improve the proposed empirical model.

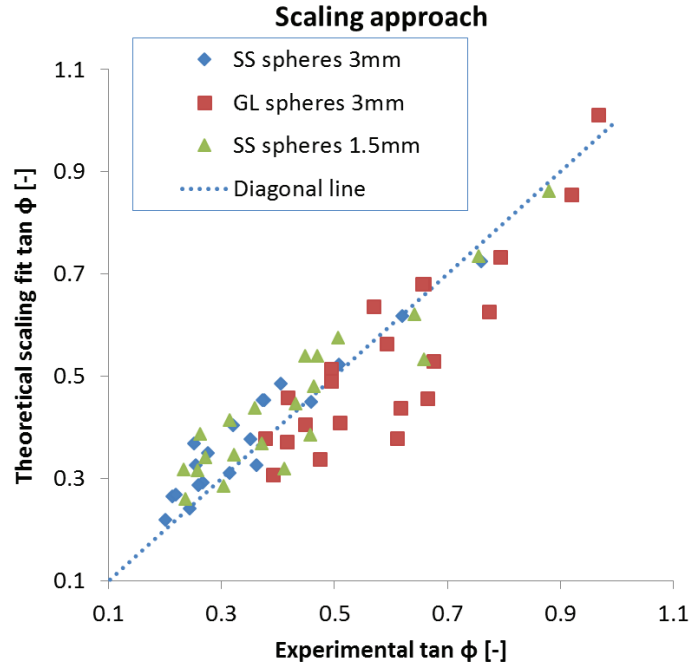


Figure 13: Validation of the scaling fit against experimental data.

4 CONCLUSIONS

Experimental data on particulate debris spreading driven by large scale turbulent flows in the pool are reported. The work is motivated by the need to provide separate effect validation data for the models which can assess effectiveness of the spreading of fragmented corium debris over the basemat area in prototypic accident severe accident conditions.

The post-test analysis of the experimental data suggests that gas injection rate in the pool, pool dimensions and particle properties have strong influence on debris bed formation. The empirical scaling for generalization of the data has been proposed. Its validation against experimental findings is in good agreement. Further experimental work is required in order to develop a database on particle spreading in the pool with wide ranges of pool configuration, particle properties and debris release conditions. Improved scaling, such as inclusion of the bubble-particle interaction into scaling expression, might be helpful for further generalization of the data.

NOMENCLATURE

α	Total void fraction in the pool
α_{eff}	Effective void fraction in the pool
a_i	Area of the i^{th} catcher
A_{tot}	Total area available at the pool bottom for particle spreading
c	Center gas injection in the pool, used in test numbering as NOPc
C_d	Drag coefficient for particle
d_p	Particle diameter (effective)

ϕ	Effective or average particle spreading angle
GL	Glass material, used in test numbering
H_{pool}, H_p, H	Pool depth (height)
L_{pool}, L_p, L	Pool length
m_i	Mass of the particulate material found in i^{th} catcher
\tilde{m}_i	Dimensionless mass fraction per area of the material found in i^{th} catcher
M_{tot}	Total mass of the particulate material
NOP	No particles of particle-free test, used in test numbering.
Q_g	Gas mass flow rate
ρ'_c	Modified density of water (coolant)
ρ_p	Density of the particulate material
R_c	Debris bed center of mass
R_{spr}	Average horizontal spreading distance for particles
RV	Reactor vessel
r_i	i^{th} catcher position measured from the gas injection chamber
s	Side gas injection in the pool, used in test numbering as NOPs, Ss or GLs
SA	Severe accident
SS	Stainless steel material, used in test numbering
$U_{g,sf}$	Gas superficial velocity
U_t	Terminal velocity of the particle

ACKNOWLEDGMENTS

The work is supported by the Swedish Nuclear Radiation Protection Authority (SSM), Swedish Power Companies, Nordic Nuclear Safety Program (NKS), Swiss Federal Nuclear Safety Inspectorate (ENSI) under the APRI–MSWI program at the Royal Institute of Technology (KTH), Stockholm, Sweden.

REFERENCES

- [1] S. E. Yakush, N. Lubchenko and P. Kudinov, "Risk-Informed Approach to Debris Bed Coolability Issue," in *Proceedings of the 20th International Conference on Nuclear Engineering (ICONE-20)*, Anaheim, California, USA, Paper 55186, July 30-August 3, (2012).
- [2] S. E. Yakush and P. Kudinov, "Simulation of Ex-Vessel Debris Bed Formation and Coolability in a LWR Severe Accident," OECD/NEA Workshop on Implementation of Severe Accident Management (SAM) Measures (ISAMM-09), Schloss Böttstein, Switzerland, CD-ROM, (2009).
- [3] E. Takasuo, T. Kinnunen, P. H. Pankakovski and S. Holmström, "The COOLOCE particle bed coolability experiments with a conical geometry: Test series 6 and 7," VTT, ID VTT-R-07097-11, Finland, (2011).
- [4] S. E. Yakush och P. Kudinov, "Effects of Water Pool Subcooling on the Debris Bed Spreading by Coolant Flow," i *Proceedings of the 11th International Conference on Advanced Nuclear Power Plants (ICAPP 2011)*, Paper 11416, Nice, France, May (2011).
- [5] N. Zhang, T. Harada, D. Hirahara, T. Matsumoto, K. Morita, K. Fukuda, H. Yamano, T. Suzuki and Y. Tobita, "Self-Leveling Onset Criteria in Debris Beds," *J. Nuclear Science and Technlogy*, vol. 47, p. 384, (2010).
- [6] N. Zhang, T. Harada, D. Hirahara, T. Matsumoto, K. Morita, K. Fukuda, H. Yamano, T. Suzuki and Y. Tobita, "Experimental investigation on self-leveling behavior in debris beds," *Nuclear Engineering and Design*, vol. 241, no. 1, p. 366, (2011).

- [7] S. Cheng, H. Tagami, H. Yamano, T. Suzuki, Y. Tobita, B. Zhang, T. Matsumoto and K. Morita, "Evaluation of debris bed self-leveling behavior: A simple empirical approach and its validations," *Annals of Nuclear Energy*, vol. 63, p. 188, (2014).
- [8] A. Konovalenko, S. Basso and P. Kudinov, "Experimental and Analytical Study of the Particulate Debris Bed Self-leveling," in *The 9th International Topical Meeting on Nuclear Thermal-Hydraulics, Operation and Safety (NUTHOS-9)*, Kaohsiung, Taiwan, September 9-13, (2012).
- [9] S. Basso, A. Konovalenko and P. Kudinov, "Development of scalable empirical closures for self-leveling of particulate debris bed," in *Proceedings of ICAPP-2014*, Charlotte NC, USA, Paper 14330, April 6-9, (2014).
- [10] S. Basso, A. Konovalenko and P. Kudinov, "Sensitivity and uncertainty analysis for predication of particulate debris bed self-leveling in prototypic Severe Accident (SA) conditions," in *Proceedings of ICAPP 2014, Paper 14329*, Charlotte, USA, April 6-9, (2014).
- [11] A. Konovalenko, S. Basso and P. Kudinov, "Experiments and Characterization of the Two-Phase Flow Driven Particulate Debris Spreading in the Pool," in *The 10th International Topical Meeting on Nuclear Thermal-Hydraulics, Operation and Safety (NUTHOS-10)*, Okinawa, Japan, (December 14-18, 2014).